Plasma Chem Plasma Process (2013) 33:1137–1152
DOI 10.1007/s11090-013-9477-1

ORIGINAL PAPER

Surface Modification of Absorbable Magnesium Stents by Reactive Ion Etching

E. Galvin · M. M. Morshed · C. Cummins · S. Daniels · C. Lally · B. MacDonald

Received: 7 May 2013 / Accepted: 7 August 2013 / Published online: 14 August 2013

Abstract The surface texture and chemistry of WE43 absorbable magnesium stents (AMS) and tube specimens processed by chemical and reactive ion etching (RIE) were investigated. Tube specimens were produced in three different conditions, namely as-received, chemically etched and plasma etched. The results of scanning electron microscopy, atomic force microscopy and energy dispersive X-ray spectroscopy studies showed that plasma etching and cleaning reduced surface roughness by 10 % compared to chemical etching alone, and completely removed surface deposits remaining from the chemical etch process. The same combination of chemical and plasma etching processes was employed to produce AMS. Expansion tests demonstrated uniform stent expansion characteristics and confirmed the viability of the device. The results of this study show that RIE is an effective surface modification technique for absorbable magnesium devices.

Keywords Reactive ion etching (RIE) · Plasma etching · Chemical etching · Magnesium alloy WE43 · Absorbable stents

Introduction

In recent times the application of gas plasma technology has grown significantly in a host of fields including the life sciences, healthcare industry and in medical device

E. Galvin (✉) · C. Lally · B. MacDonald
School of Mechanical and Manufacturing Engineering, Dublin City University, Dublin 9, Ireland
e-mail: emmet.galvin3@mail.dcu.ie

M. M. Morshed · S. Daniels
National Centre for Plasma Science and Technology (NCPST),
Dublin City University,
Dublin 9, Ireland

C. Cummins
Vasorum Ltd., 2012 Orchard Avenue, Citywest Campus, Dublin 24, Ireland

manufacturing. Gas plasma disinfection systems have demonstrated many advantages over more conventional methods for preventing hospital-acquired infections [1]. In medical device manufacturing, gas plasma processes offer reliable and repeatable surface modification and sterilisation techniques for devices with complex shapes, such as intravascular stents. Gas plasma provides multiple surface modification options, such as conformal and defect-free coatings with unique chemistry and excellent adhesion properties, permeation barriers with low levels of leaching and sterile and activated (hydrophilic and hydrophobic) surfaces [2]. Plasma etching removes manufacturing residues, foreign materials and bioburden and offers a clean, safe and environmentally-friendly alternative to traditional wet chemical processes. The sterilisation of medical devices by plasma processes has several advantages over conventional sterilisation techniques (autoclaving, γ-radiation, hydrogen peroxide and ethylene oxide), including low cost, short treatment times, the ability to treat heat-sensitive materials and the absence of humidity and toxic residues [3–5]. These numerous capabilities make gas plasma processes particularly useful in the manufacture of stents.

The implantation of intravascular stents is one of the most commonly used treatments for coronary artery disease [6]. Stents are cylindrical mesh structures that are expanded at the blockage site in order to deform the stenosis and scaffold it against the walls of the vessel, thus restoring blood flow [7]. Many contemporary intravascular stents are manufactured as permanent implants from materials such as stainless steel, cobalt chromium, tantalum and titanium. These devices are designed to remain inert in the in vivo environment. Limitations in mechanical properties and biocompatibility, and the on-going presence of the device can result in a host of adverse reactions and chronic conditions in the vasculature, such as adverse remodelling phenomena and in-stent restenosis [8]. Consequently, intravascular stent technology has progressed toward the development of absorbable stents that temporarily scaffold the vessel during the initial period of high risk for recoil, and then degrade in the long term [9]. A number of absorbable materials have been proposed including polymers such as poly-L-lactic-acid (PLLA) [10, 11], iron-based alloys [12, 13] and magnesium alloys [14–17]. Magnesium is an outstanding candidate material for absorbable stents as it has suitable mechanical properties, good biocompatibility, favourable corrosion kinetics and can provide a platform for drug delivery systems. There is little information available in the published literature however, with regard to the manufacture of absorbable magnesium stents [15, 18–20]. Fibre laser cutting of stents from tubes of the AZ31 magnesium alloy has been reported [19, 20]. However, no such study has been reported for the laser cutting of stents from tubes of the WE43 magnesium alloy. The WE43 alloy was used in the manufacture of the Biotronik AMS platform and is presently the only magnesium stent platform to successfully go through clinical trials for coronary [21–23] and peripheral [24, 25] applications.

Currently, stents sculpted by laser machining require further postprocessing in order to produce the required geometry and surface texture. The quality of the stent surface is of great concern as it significantly influences device biocompatibility. Typically a laser cut stent will pass through additional processing steps including, but not limited to, acid pickling or soft etching, annealing, electropolishing, passivation and sterilisation [26]. Plasma and ion beam technologies offer effective methods for surface modification of medical implants, such as stents. A number of studies have reported plasma-immersion ion implantation of magnesium surfaces using nitrogen, aluminium and oxygen (O_2) in order to improve the corrosion resistance of biomedical and automotive components [27–30]. To the authors' knowledge this is the first study to report the surface modification of AMS by reactive ion etching. In this context, AMS were manufactured from tubes of the WE43 magnesium alloy by pulsed fibre laser

machining. The stents were postprocessed by a combination of chemical and plasma etching processes. Chemical etching removed the bulk dross and spatter that remained from the laser cutting process. Plasma etching in argon-oxygen ($Ar–O_2$) gas mixture, followed by plasma cleaning in pure O_2, removed surface deposits that remained from the chemical etching process and completely cleaned the stent surfaces. Expansion experiments demonstrated uniform stent expansion characteristics and confirmed the viability of the stents manufactured.

Materials and Methods

Stent Manufacture and Testing

AMS were manufactured from tubes of the WE43 magnesium alloy. The WE43 alloy contained approximately 93 % magnesium, <4 % yttrium (Y), 0.7 % zirconium (Zr), and the remainder consisted of rare-earth (RE) elements [Neodymium (Nd), Gadolinium (Gd), Dysprosium (Dy), Erbium (Er) and Ytterbium (Yb)]. The tubes had an outer diameter (OD) of 2.1 mm and a wall thickness of 0.15 mm.

The stent design was approximated from published images of the Biotronik AMS-1 platform [15]. The unfurled stent geometry was first modelled in a computer-aided design (CAD) software package (SolidWorks Corp., MA, USA), as shown in Fig. 1a. The CAD data were then used to produce a computer numerical control (CNC) program that defined all cutting paths necessary to sculpt the stent by pulsed fibre laser machining. The laser beam had a wavelength of 1,070 nm and width of 13 μm. Argon (Ar) was employed as an inert shield gas. The finished AMS had an overall length of 11.94 mm, OD of 2.09 mm, wall thickness of 0.14 mm and a strut width of 0.12 mm. Figure 1b shows a scanning electron microscopy (SEM) image of a tube in which the stent pattern was machined. Figure 2a shows the stent after the inner sections were removed. Figure 2b shows a significant amount of dross and spatter adherence on the inner surface of the struts which was subsequently removed by a combination of chemical and plasma etching processes.

Chemical Etching

A chemical etching process was employed to remove the bulk dross, spatter and heat-affected zone (HAZ) that formed during laser cutting. This process also rounded-off strut edges and

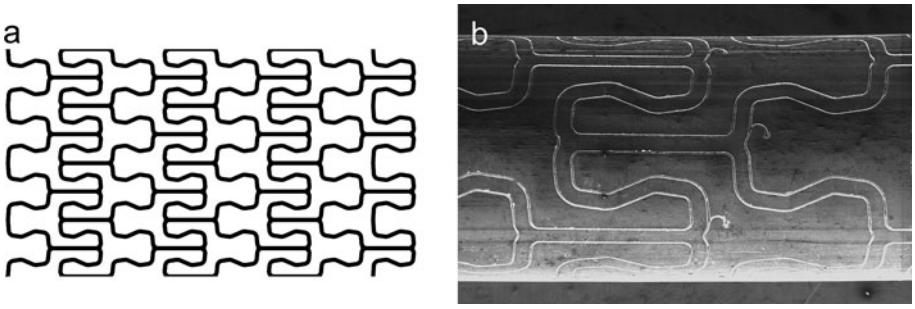

Fig. 1 **a** Two-dimensional CAD model of the unfurled stent geometry, and **b** SEM image of a tube in which the stent pattern was machined

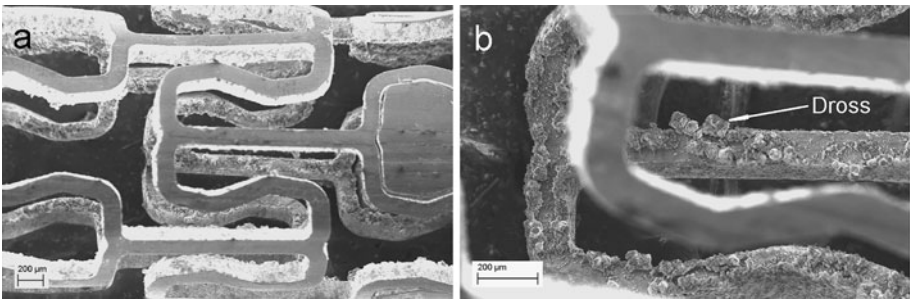

Fig. 2 **a** Machined stent remaining after the inner sections had fallen out, and **b** dross that formed on the inner surface of the stent as a result of laser cutting process

improved the surface finish and stent deployment characteristics. The stents were chemically etched in 85.2 % phosphoric acid (P6560, Sigma Aldrich) at 55 °C for 20 s and then neutralised immediately by immersion in sodium hydroxide solution (100 g/L, S8045, Sigma Aldrich) for 30 s at room temperature. The stents were sonicated in ultrapure H_2O for 2 min, followed by 100 % industrial methylated spirits (IMS) for a further 2 min. Specimens were dried for 2 h in a cleanroom environment (class 100) using a glass drying oven (B-585, BUCHI Labortechnik AG) and an air temperature of 25 °C [31].

Plasma Etching

In order to remove residues remaining from the chemical etching process the stents were placed in the chamber of a RIE instrument (PlasmaLab 80 Plus, Oxford Instruments). Figure 3 shows a schematic diagram of the experimental setup used for the plasma etching process. As RIE acts mainly as a "line-of-sight" process, etching was performed in three stages where the specimens were manually rotated in increments of 120° on a quartz plate in order to minimise shadowing effects. A capacitively coupled plasma was generated by a 13.56 MHz radio-frequency (RF) power source. The RF powered electrode was made from stainless steel and had an outer diameter of 240 mm. The grounded electrode was made from stainless steel and acted as a showerhead to supply the process gases. The distance between the powered and grounded electrodes was 46 mm. Plasma etching was performed in two separate process steps using two different process gases. In the first step, the surface of the stents were plasma etched in a mixture of 90 % Ar and 10 % O_2 gas for a total of 10 min. The comparatively heavy Ar ions removed material by a micro-sandblast effect upon striking the substrate. In the second step, the stents were cleaned and sterilised in 100 % O_2 gas for a further 10 min. O_2 plasma reacts with molecules deposited on the substrate breaking them down and turning them into volatile compounds. In both cases the process conditions were kept constant where the chamber pressure was 100 mTorr, the power was 250 W and the flow of gas was 100 sccm. A bias voltage of $\sim$495 V was recorded.

Stent Expansion Test

Experiments were carried out in order to assess the expansion performance of a total of three stents. In each test, a stent was mounted in the uncrimped state on a 3.5 $\times$ 30 mm angioplasty balloon and inflated to a maximum pressure of 15 atmospheres using a Merit

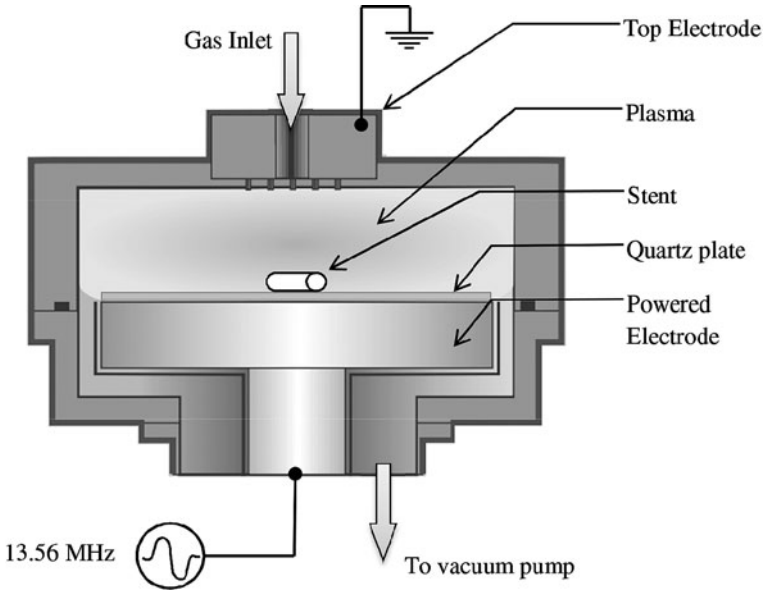

Fig. 3 Schematic diagram of the experimental setup for plasma etching process

Medical Basix-T Compak® inflation device. The balloon was then deflated and the stents were permitted to undergo elastic recoil. A video-extensometer was used to record calibrated images of the stent expansion procedure (Messphysik MTV-13W1C, Mintron Enterprise Co. Ltd.). Elastic radial recoil (ERR) was calculated according to the formula previously described by Migliavacca et al. [32]. The surfaces of the expanded stents were examined for signs of fracture and other defects using a SEM (Leo 440 Stereo scan, Leica Microsystems). The uncoated specimens were examined using an accelerating voltage of 5 kV and a chamber pressure of 2.0×10^{-6} mbar.

Specimen Preparation and Analysis

Test specimens with a length of 10 mm were cut from the WE43 tube, then degreased by sonication in alcohol (100 % IMS) and finally placed in a glass drying oven for 2 h at 25 °C. Specimens were prepared in three different conditions, namely as-received, chemically etched and plasma etched. Tube specimens were subjected to the same chemical and plasma etching processes that were used to produce the stents. SEM, atomic force microscopy (AFM) and energy dispersive X-ray spectroscopy (EDX) analyses were performed on the tube specimens in order to characterise the morphology, roughness and chemical composition of surfaces for the three different conditions.

EDX Analysis

Prior to EDX analysis all specimens were sputter coated with a thin film of carbon in order to render them conductive. EDX analysis was performed using an INCA Energy 350 XT microanalysis system (Oxford Instruments) in conjunction with a Leo 440 Stereo scan SEM. The vacuum in the chamber was 2.0×10^{-6} mbar. The beam current and spot size

of the electron gun was set to 1.0 nA and 520 nm, respectively. The working distance between the specimen and electron gun was maintained between 8.5 and 9 mm and the collection time for the EDX detector was 120 s. Quantitative EDX analysis was performed using the INCA Microanalysis Suite (v4.09) software package. Background correction was performed using the background modelling method where the detector background spectrum was subtracted from the observed spectral distribution by mathematical filtering using a top hat function. The intensity of spectral peaks corresponding to specimen elements were measured and compared to standards measured under known operating conditions by the software. Intensity ratios (k values) were calculated and converted into chemical concentration (wt%) for the elements detected within the specimen.

Surface Roughness Analysis

The surface texture of treated and untreated specimens was scanned using high resolution contact mode AFM (Nano-R^{TM} O-020, Pacific Nanotechnology). A cantilever AFM tip (SICON-10P, Applied NanoStructures, Inc.) was drawn along the outer surface of each specimen in the longitudinal direction. Three randomly selected regions, measuring 80 μm × 80 μm, were scanned on each specimen. The scan rate and number of lines in each scan were kept constant at 0.5 Hz and 256, respectively. The surface roughness parameter (Sa) was calculated without a filtering process using the SPM Cockpit^{TM} (V3.3.383) software package according to the formula listed in ASME B46.1. A one-way analysis of variance (ANOVA) was used to test for differences among the surface roughness values (Sa) of the three specimen groups (as-received, chemically etched and plasma etched).

Results and Discussion

Stent Manufacture

Laser Cutting

Many challenges exist in the laser cutting of stents where inconsistency in the geometry of the struts can result in reduced stent expansion performance. The effectiveness of laser cutting is greatly influenced by the physical properties of the material to be machined. Magnesium alloys possess many inherent characteristics that render them difficult to machine by laser such as low absorptivity of laser light, a strong tendency to oxidise and to form low melting-point constituents, high thermal conductivity and high coefficient of thermal expansion, high solubility for hydrogen in the liquid state and a wide solidification temperature range [33]. Consequently, processing problems can be encountered such as formation of dross, burrs and spatter, porous oxide inclusions, loss of alloying elements, excessive pore formation, recast layer, striations, backwall damage and liquation and solidification cracking.

Laser cutting of WE43 tubes produced parts with substantial dross and spatter attachment, as shown in Fig. 2. Dross can form during laser cutting when a significant temperature gradient exists between the top and bottom surface of the work-piece. Divergence of the laser beam results in a larger kerf width as a greater amount of material is melted on the underside of the work-piece. The low viscosity and low surface tension of melted magnesium contributed to the large amounts of spatter attachment. Excessive amounts of

dross and spatter attachment on the inner surface of the tube prevented the normal fallout of cut sections.

Machining parameters were optimised for cutting the WE43 material including the laser power, pulse duration, cutting speed and repetition rate. Ar was selected as an inert shield gas in order to minimise oxidation and gas pressure was increased to improve the quality of the cut and to reduce dross accumulation. The focal position of the laser beam was adjusted to increase the kerf width and hence aid fallout of cut sections. Optimisation of laser parameters successfully reduced dross and spatter adherence. The remaining dross was removed by a combination of chemical and plasma etching processes.

Etching and Cleaning

There was an observable difference in the surface texture of inner, outer and laser cut stent surfaces. The difference in texture of inner and outer surfaces appeared to originate from the drawing process employed to produce the tubes. Outer surfaces had the smoothest appearance while inner surfaces appeared rougher. Surfaces produced by laser cutting had the roughest appearance. Chemical etching with phosphoric acid removed bulk dross and surface scale from all stent surfaces. The texture of all stent surfaces was significantly improved to a more uniform morphology, as shown in Fig. 4. Significant variation was evident in the surface texture of inner, outer and laser cut surfaces after chemical etching. Phosphoric acid etching formed a non-toxic and corrosion-resistant magnesium phosphate surface layer [34]. However, a significant amount of residue and contamination remained on the stent surfaces following the chemical etching process, as shown in Fig. 4.

Plasma etching and cleaning was employed to remove surface deposits and contamination remaining from the chemical etching process. SEM images of a finished magnesium stent are shown in Fig. 5. It can be seen that plasma etched surfaces appeared lighter in colour compared to chemically etched surfaces and residues were completely removed. Plasma processing reduced surface roughness of all surfaces compared to chemically etched surfaces. The plasma etching process was most effective on the outer surface and less effective on shadowed surfaces and laser cut edges, see Fig. 5. Plasma etching was performed in three stages where the specimens were manually rotated in increments of 120° on the quartz plate in order to minimise shadowing effects. Although RIE acts mainly as a "line-of-sight" process, it is likely that a significant number of ions would have reached the inner stent surfaces owing to the small strut width (120 μm), the comparatively large spacing between the struts, and the high sheath potential (~495 V). The specimen

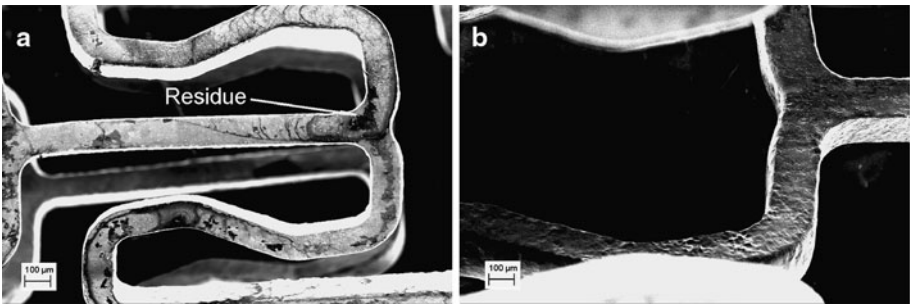

Fig. 4 Stent surfaces resulting from chemical etching. **a** *Outer* stent surface with residue (*dark areas*), and **b** *inner* surface of stent strut

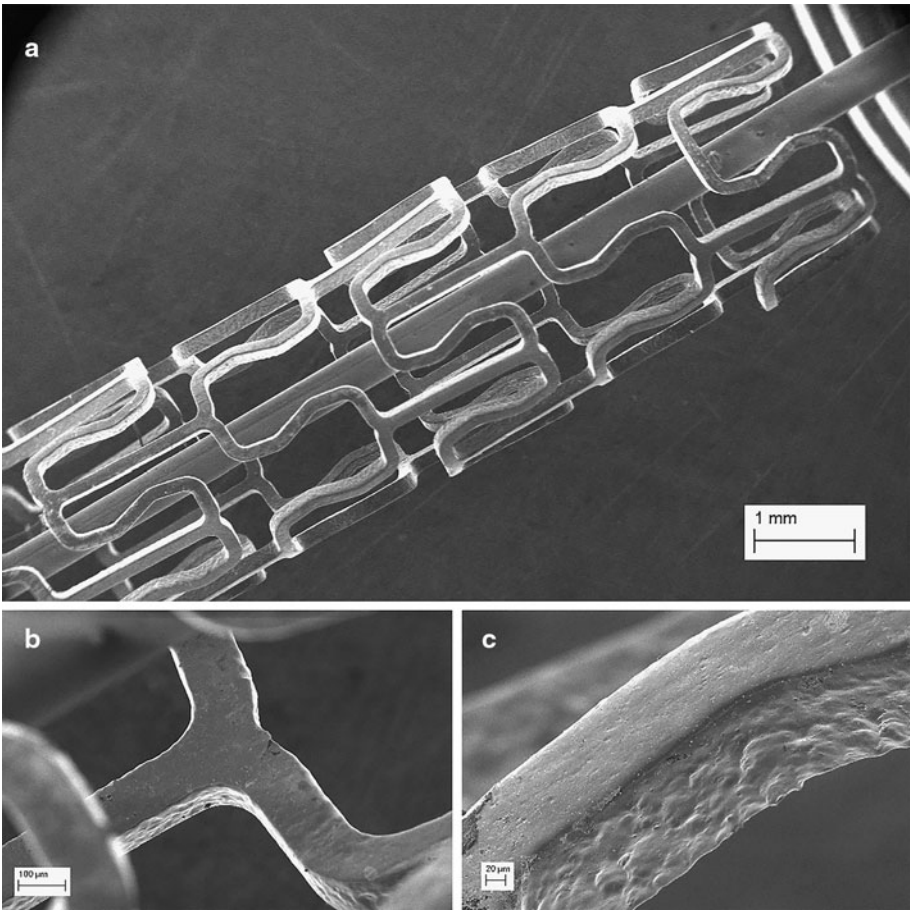

Fig. 5 SEM images of finished stent following plasma etching and cleaning. **a** Stent mounted on fused silica tube, **b** *inner* surface, and **c** *outer* surface

rotation technique employed here would have limited efficacy in reducing the shadowing effects. A planetary rotating system would provide a more effective method to minimise shadowing effects through continuous specimen rotation during plasma processing.

The etch rate of the 90 % Ar and 10 % O_2 plasma process was not measured as it was beyond the scope of this work. However, one would expect a significantly higher etch rate for the WE43 alloy when compared to harder biomaterials such as 316L stainless steel, cobalt-chromium alloys and titanium alloys. Etch rates of 20–30 nm/min in 100 % Ar plasma have been reported for pure magnesium [35] and magnesium oxide (MgO) thin films [36]. These studies used higher power settings (300–500 W) and higher proportions of Ar compared to those used in this work. Increased etch rates can be expected for increasing power, increasing proportion of Ar gas and decreasing chamber pressure. Increasing power increases the formation of Ar ions within the plasma. This results in more bombardment of the surface and a greater etch rate. The use of comparatively lower power settings and a lower proportion of Ar suggest etch rates well below 20 nm/min for the

WE43 alloy material. Therefore, one may expect that a layer of material no more than 0.3 μm thick was removed from the AMS with a processing time of 10 min.

EDX Analysis

Figure 6a shows that as-received specimens had a relatively rough surface morphology that consisted mainly of a dark-coloured magnesium (Mg) matrix area (alpha (α) phase) interspersed with lighter-coloured beta (β) phase areas [37]. The chemical compositions of both the α-phase and β-phase regions of the specimen were measured by EDX at three different sites. Figure 6a shows the sites where spectra were taken for α-phase (S1–S3) and β-phase (S4–S6) measurements. The weight percent (%) of each element detected at the three sites was averaged (mean) in order to produce the plot shown in Fig. 6b. The error bars were calculated as the standard deviation in order to represent the overall distribution of the data. EDX analysis confirmed the α-phase had high concentrations of Mg (62 %) and low concentrations of distributed alloying elements Y (5.6 %), Nd (6.2 %) and Zr (1.0 %) along with O_2 (19.4 %) and C (6.1 %). Conversely, the surface of the secondary phase areas had low Mg (16.7 %) and relatively higher concentrations of alloying elements Y (19.6 %), Nd (30.3 %) and Zr (1.3 %) along with O_2 (28.3 %) and C (4.0 %).

Chemical etching in phosphoric acid resulted in significant changes in the appearance and surface chemistry of the specimens. The native oxide layer was replaced with a more passive oxide layer with lower porosity and increased corrosion resistance. The surface morphology was more homogenous owing to the lower porosity of the new oxide layer, as shown in Fig. 7a. EDX analysis showed that the new surface layer consisted of Mg (91.3 %), Y (0.8 %), Zr (0.1 %), O_2 (6.0 %) and C (0.6 %) and small amounts of Na (1.0 %) and P (0.1–0.85 %). It is believed that the presence of P in the surface layer can be attributed to the formation of magnesium phosphate during etching [34]. The presence of Na in the surface layer may be attributed to the formation of a thin layer of sodium hydroxide that is adsorbed to the specimen during the neutralisation treatment. A number of rectangular-shaped entities were distributed within the surface layer of chemically etched specimens, as shown in Fig. 7a. An EDX spectrum at S2 showed that these entities were rich in the RE elements Y (80.3 %), Nd (9.9 %) and Zr (0.8 %). The dark surface

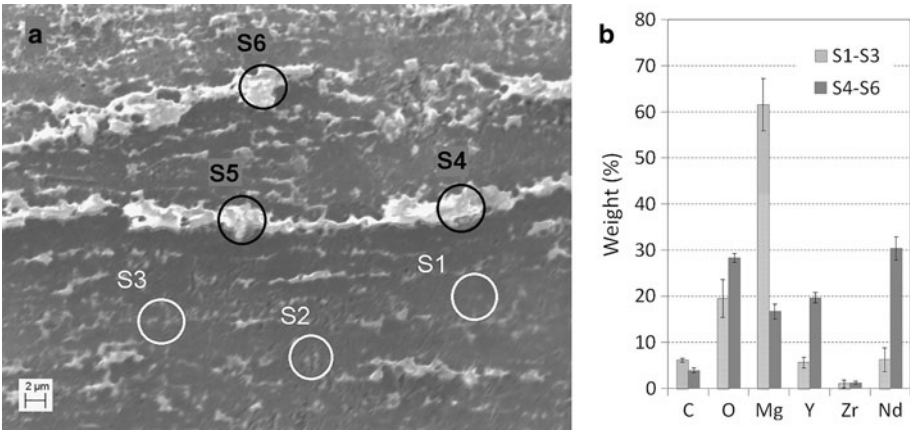

Fig. 6 **a** Typical surface morphology of as-received specimen showing spectra sites S1–S6, and **b** average chemical composition at spectra sites S1–S3 and spectra sites S3–S6

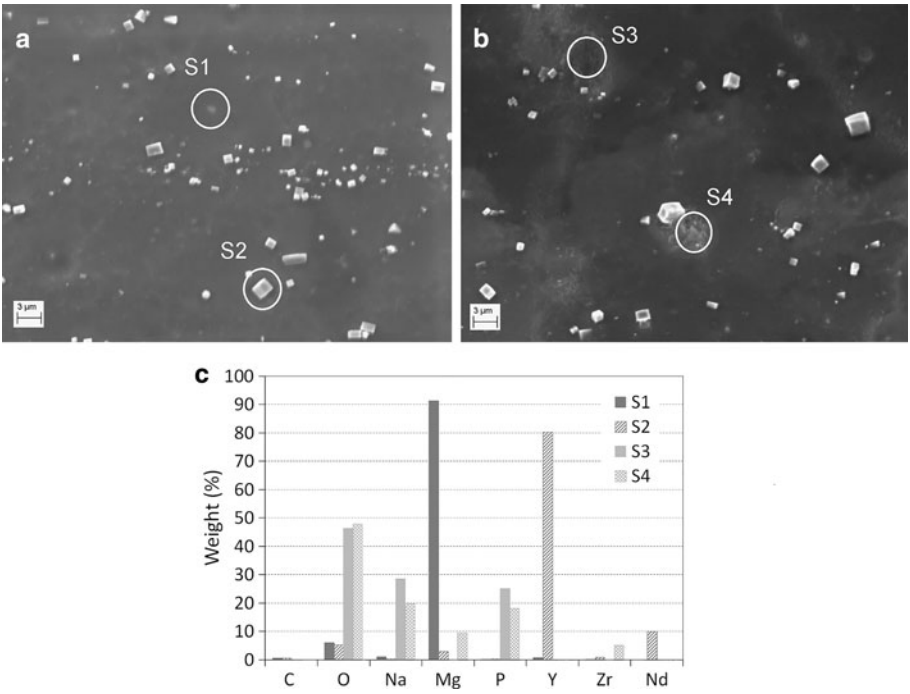

Fig. 7 Typical surface morphology of chemically etched specimen. **a** Normal surface appearance, **b** *dark area* with surface residue, and **c** chemical composition of surface at spectra sites S1–S4

deposits shown in Fig. 7b consisted mainly of O_2 (46–48 %), Na (19.7–28.5 %), P (18–25.1 %) and Mg (1–10 %). These heavy deposits are likely to be oxides with P and NaOH content. This would likely explain the high O_2 content observed at these sites.

Plasma etching successfully removed all unwanted surface deposits and residue. Further, many of the RE-rich entities that remained on the surface after chemical etching were reduced in size or completely removed from the surface, as shown in Fig. 8a. The underlying material phases were more visible after plasma etching. EDX analysis showed lower concentrations of P and Na on plasma etched surfaces compared to chemically etched surfaces, as shown in Fig. 8b. These results suggest that the heavy Ar ions in the plasma removed some of the phosphor-rich coating. The amount of material removed from the surface can easily be controlled by changing the treatment time. Alternatively, plasma cleaning in reactive oxygen gas alone can provide sterile surfaces without removing the protective phosphor-rich coating.

A preliminary corrosion study in static simulated body fluid (H8264, Sigma Aldrich) was performed using a treated and an untreated AMS. The results suggest that the P-rich coating provided additional protection to the magnesium substrate up to a time of approximately 48 h when compared to the bare substrate alone. However, once the solution penetrated the P-rich coating the corrosion rate accelerated dramatically and a rapid loss of mechanical integrity ensued owing mainly to intergranular corrosion. The use of plasma etching and cleaning produced a sterile surface with excellent adhesion properties. Future work will involve producing AMS with a biodegradable polymer coating that can extend the life of the device by delaying the onset of corrosion in a controlled manner [38].

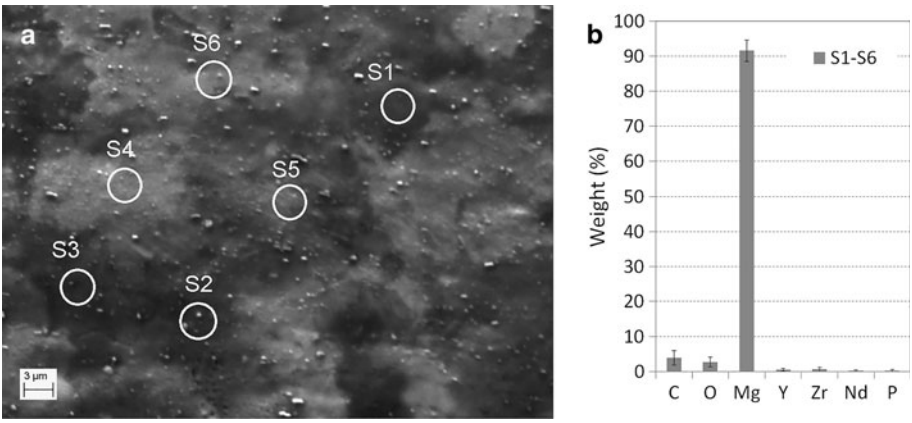

Fig. 8 **a** Typical surface morphology of plasma etched specimen showing EDX spectra sites S1–S6, and **b** average chemical composition of surface at spectra sites S1–S6

The coating should also enhance biocompatibility by limiting platelet adhesion and reactivity [39] and by providing a vehicle for the delivery of an anti-proliferative drug.

The Biotronik AMS platform demonstrated good biocompatibility for both animal tests and clinical trials [14] though the toxicology and metabolic pathway of the rare earth elements used in the WE43 alloy requires further investigation [40]. The biocompatibility of medical implants depends upon surface properties such as sterility, chemical composition, corrosion resistance, texture, wettability (contact angle), surface energy and surface charge [41]. A previous study showed that mechanically polished magnesium alloy surfaces were hydrophobic in nature with contact angle values varying between 93° and 98° [42]. The contact angle of MgO surfaces was reduced from 70° to around 10° after cleaning in O_2 plasma for 2 min [43]. An improvement in the biocompatibility of AMS may be expected owing to chemical etching in phosphoric acid which formed a non-toxic and corrosion-resistant magnesium phosphate surface layer [34] Plasma processing should enhance the biocompatibility of the surface through improvements in surface sterility, corrosion resistance and increased surface wettability (hydrophilicity). It has been shown that O_2 plasma processing of biomaterials leads to increased surface wettability [43] and enhanced adhesion properties for subsequent coating processes [44]. Future work should involve determining the influence of chemical and plasma etching processes on the various surface properties which effect biocompatibility. Biocompatibility testing should include cytotoxicity, haemolysis and platelet adhesion testing, cell viability assays and corrosion analysis.

Surface Roughness Analysis

Figure 9 shows surface morphologies measured by AFM for as-received, chemically etched and plasma etched specimens. Figure 10 shows average surface roughness values (Sa) for the same three specimen conditions. It was found that plasma etched specimens had the lowest surface roughness (172 nm) compared to chemically etched (191 nm) and as-received (223 nm) specimens. A one-way ANOVA showed that the mean surface roughness amongst the three specimen groups (as-received, chemically etched and plasma etched) was statistically significant [$F(2, 6) = 5.14$, $p = 0.006$]. As Fig. 8 shows, many of

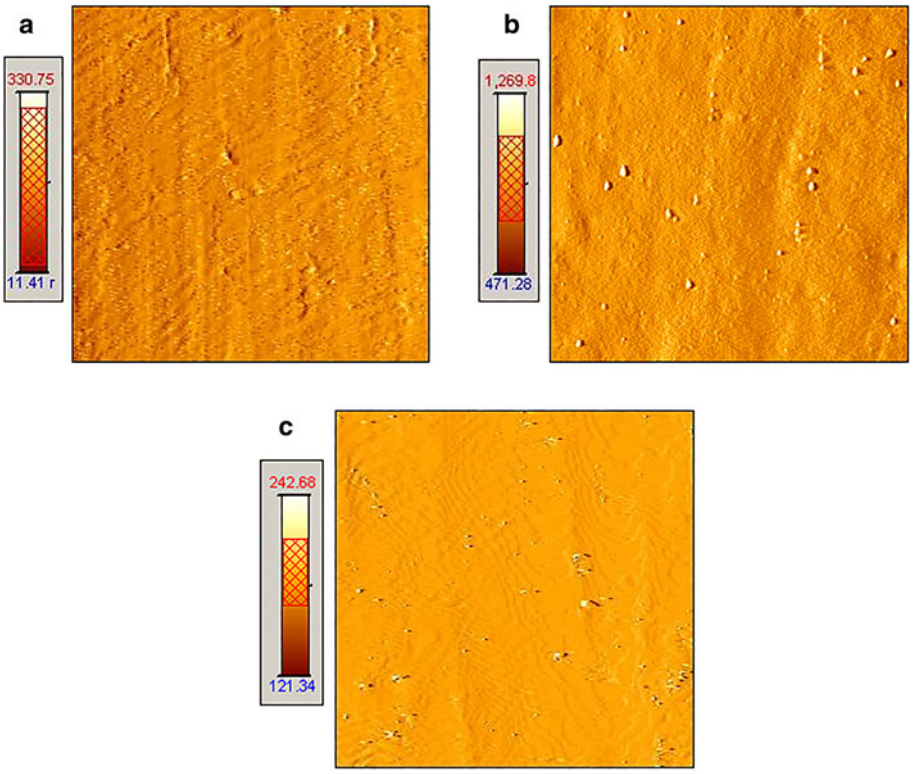

Fig. 9 Typical surface morphology of specimens generated by AFM. **a** As-received, **b** chemically etched, and **c** plasma etched

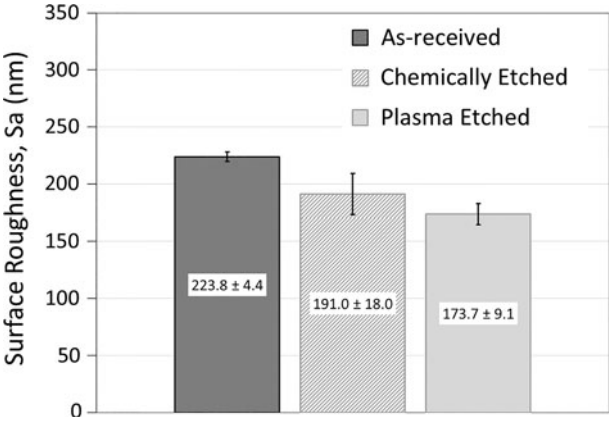

Fig. 10 Surface roughness (Sa) values (mean ± SD) measured by AFM for as-received, chemically etched and plasma etched tube specimens

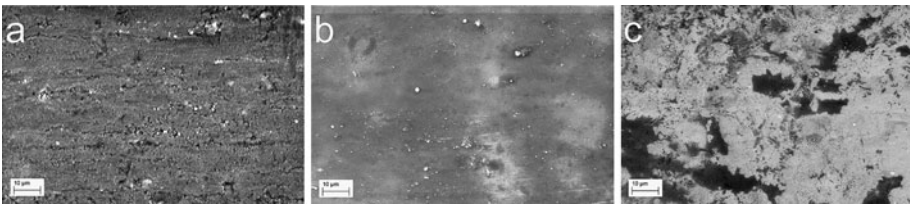

Fig. 11 SEM images of tube specimens. **a** As-received, **b** chemically etched, and **c** plasma etched and cleaned (*magnification* ×1,000)

the RE-rich entities that remained following chemical etching diminished in size or were completely removed from the surface by plasma etching. This contributed to an overall reduction in surface roughness values, as shown in Fig. 10.

The magnesium tubes used in this work were subjected to an annealing process. The average surface roughness of tubes was relatively high in the as-received condition owing to the non-uniform morphology and surface defects that remained after tube extrusion processing. Figure 11a shows the parallel lines and defects that ran longitudinally on the surface of the tube indicating the direction of the tube extrusion process. These surface defects are potential sites of stress concentrations and material failure due to crack growth during stent expansion. The combination of chemical and plasma processing steps was intended to reduce or eliminate these defects. The surface texture was considerably improved by chemical etching which reduced the average surface roughness (Sa) value by 14.7 % from 223 to 191 nm. No surface defects were evident on the phosphor-rich surface layer produced by chemical etching, as shown in Fig. 11b. The plasma etched surface was considerably brighter in appearance compared to the surfaces of the other two specimens, as shown in Fig. 11c. The average surface roughness of plasma treated specimens was 10 % lower (172 nm) compared to chemically etched specimens (191 nm).

Magnesium surfaces with low roughness are desirable for a number of reasons. It has been shown that the passivation behaviour of magnesium alloys is affected by increasing surface roughness and consequently pitting tendency and corrosion rate decrease with decreasing surface roughness [45]. The use of chemical etching and plasma etching can reduce surface roughness and improve corrosion resistance. This permits the mechanical integrity of the stent to be maintained for a longer period of time.

Stent Expansion Testing

Figure 12 shows the stent configuration at three different phases of the expansion process; (a) mounted on the balloon prior to expansion; (b) fully expanded to an average maximum OD of 4.3 mm, and (c) after elastic recoil upon balloon deflation. Average ERR was 3.5 % for the three stents tested. This figure correlated well with ERR data for commercially-available stents [46]. The expanded configuration and final OD were relatively uniform in the stent structure, as shown in Fig. 12c. This demonstrated satisfactory stent expansion characteristics.

During laser processing, thermal effects result in the formation of a HAZ at the machined edges. This can affect the stress–strain properties, yield stress and fatigue-strength of the stent. In some cases the HAZ is embrittled compared to the bulk material, resulting in micro-cracks that can propagate through the strut during stent expansion. The use of an inert shield gas, appropriate laser cutting parameters and appropriate post-processing (e.g. etching) can greatly reduce the effects of a HAZ [33]. During the stent

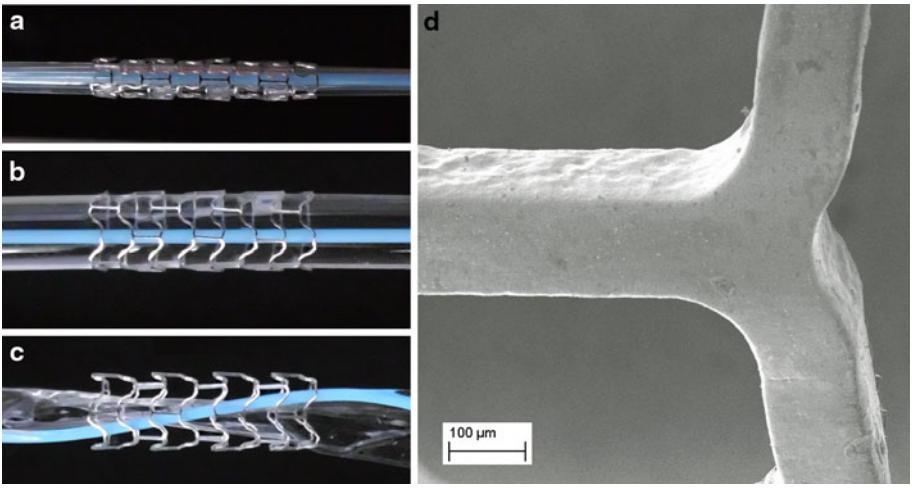

Fig. 12 Expansion testing of AMS. **a** Unexpanded, **b** fully expanded at 15 atm. Pressure, **c** after recoil, and **d** SEM image of a strut section from an expanded stent

expansion process, elevated strain levels induced at plastic hinge sites may cause cracking of the brittle surface oxide and may introduce micro-cracks and sub-surface defects into the substrate. The stents were examined after expansion using a SEM. There was no evidence of strut failure or cracking, as shown in Fig. 12d. Strut cracks are difficult to detect in post-expansion analysis (i.e. visual examination) as they are likely to close upon balloon deflation. Magnesium has high affinity to oxygen and therefore a new surface oxide is likely to quickly form over cracks and other surface defects making their detection difficult. Such sub-surface defects would likely become evident with the onset of corrosion in the magnesium substrate. Non-destructive test (NDT) methods such as ultrasonic testing (UT), eddy current (EC) or phased array (PA) could be used to determine the severity of the material damage induced by the stent expansion process.

Conclusions

Laser machining parameters were optimised for cutting the WE43 tube and for sculpting absorbable magnesium stents. A chemical etching process was used to remove bulk dross and spatter remaining from the laser cutting process. SEM, AFM and EDX studies showed that plasma etching and cleaning in a mixture of Ar-O_2 gas plasma and pure O_2 plasma successfully reduced surface roughness by 10 % compared to chemically etched surfaces and completely removed surface contaminants remaining from the chemical etch process. Chemical and plasma etching processes can reduce surface roughness and improve the corrosion resistance of magnesium alloy surfaces. This permits the mechanical integrity of stents and other implants to be maintained for a longer period of time. The deployment characteristics of the stents produced was shown to be satisfactory in stent expansion experiments. The average ERR of the stent was comparable to that of commercially-available stents. The results of this study demonstrate that RIE is an effective surface modification technique for magnesium alloy medical devices.

Acknowledgments The authors would like to acknowledge the provision of project funding by an IRC-SET fellowship under the Embark Initiative (RS/2006/82).

References

1. Cotter JJ, Maguire P, Soberon F et al (2011) Disinfection of meticillin-resistant Staphylococcus aureus and *Staphylococcus epidermidis* biofilms using a remote non-thermal gas plasma. J Hosp Infect 78:204–207
2. Yang J, Cui F, Lee IS, Wang X (2010) Plasma surface modification of magnesium alloy for biomedical application. Surf Coat Technol 205:S182–S187
3. Cvelbar U, Vujoševič D, Vratnica Z, Mozetič M (2006) The influence of substrate material on bacteria sterilization in an oxygen plasma glow discharge. J Phys D Appl Phys 39:3487–3493
4. Halfmann H, Bibinov N, Wunderlich J, Awakowicz P (2007) A double inductively coupled plasma for sterilization of medical devices. J Phys D Appl Phys 40:4145–4154
5. Moreira AJ, Mansano RD, Andreoli Pinto TDJ et al (2004) Sterilization by oxygen plasma. Appl Surf Sci 235:151–155
6. Serruys PW (2006) Fourth annual American College of Cardiology international lecture: a journey in the interventional field. J Am Coll Cardiol 47:1754–1768
7. Lally C, Kelly DJ, Prendergast PJ (2006). Stents. Wiley Encyclopedia of Biomedical Engineering. doi: 10.1002/9780471740360.ebs1142
8. Serruys PW, Ormiston JA, Onuma Y et al (2009) A bioabsorbable everolimus–eluting coronary stent system (ABSORB): 2-year outcomes and results from multiple imaging methods. Lancet 373:897–910
9. Erne P, Schier M, Resink TJ (2006) The road to bioabsorbable stents: reaching clinical reality? Cardiovasc Intervent Radiol 29:11–16
10. Stack RE, Califf RM, Phillips HR (1988) Interventional cardiac catheterization at Duke Medical Center. Am J Cardiol 62:3F–24F
11. Tamai H, Igaki K, Kyo E et al (2000) Initial and 6-month results of biodegradable poly-L-lactid acid coronary sents in humans. J Am Heart Assoc 102:399–404
12. Peuster M, Wohlsein P, Brugmann M et al (2001) A novel approach to temporary stenting: degradable cardiovascular stents produced from corrodible metal-results 6–18 months after implantation into New Zealand white rabbits. Heart (Br Card Soc) 86:563–569
13. Peuster M, Hesse C, Schloo T et al (2006) Long-term biocompatibility of a corrodible peripheral iron stent in the porcine descending aorta. Biomaterials 27:4955–4962
14. Heublein B, Rohde R, Kaese V et al (2003) Biocorrosion of magnesium alloys: a new principle in cardiovascular implant technology? Heart 89:651–656
15. Di Mario C, Griffiths H, Goktekin O et al (2004) Drug-eluting bioabsorbable magnesium stent. J Interv Cardiol 17:391–395
16. Peeters P, Bosiers M, Verbist J et al (2005) Preliminary results after application of absorbable metal stents in patients with critical limb ischemia. J Endovasc Ther 12:1–5
17. Hermawan H, Alamdari H, Mantovani D, Dubé D (2008) Iron–manganese: new class of metallic degradable biomaterials prepared by powder metallurgy. Powder Metall 51:38–45
18. Hassel T, Bach FW, Golovko AN (2006) Production and properties of small tubes made from MgCa0.8 for application as stent in biomedical science. In: Kainer KU (ed) 7th international conference on magnesium alloys and their applications. Wiley-VCH, Dresden
19. Demir AG, Previtali B, Colombo D et al (2012) Fiber laser micromachining of magnesium alloy tubes for biocompatible and biodegradable cardiovascular stents. In: Proceedings of the SPIE, vol 8237
20. Wu W, Chen S, Gastaldi D, Petrini L (2012) Experimental data confirm numerical modeling on degradation process of magnesium alloys stents. Acta Biomater (in press)
21. Waksman R, Erbel R, Di Mario C et al (2009) Early- and long-term intravascular ultrasound and angiographic findings after bioabsorbable magnesium stent implantation in human coronary arteries. JACC Cardiovasc Interv 2:312–320
22. Erbel R, Di Mario C, Bartunek J et al (2007) Temporary scaffolding of coronary arteries with bioabsorbable magnesium stents: a prospective, non-randomised multicentre trial. Lancet 369:1869–1875
23. Haude M, Erbel R, Erne P et al (2013) Safety and performance of the drug-eluting absorbable metal scaffold (DREAMS) in patients with de-novo coronary lesions: 12 month results of the prospective, multicentre, first-in-man BIOSOLVE-I trial. Lancet 6736:1–9
24. Bosiers M, Deloose K, Verbist J, Peeters P (2005) First clinical application of absorbable metal stents in the treatment of critical limb ischemia: 12-month results. Vasc Dis Manag 2:86–91

25. Bosiers M, Peeters P, D'Archambeau O et al (2009) AMS INSIGHT—absorbable metal stent implantation for treatment of below-the-knee critical limb ischemia: 6-month analysis. Cardiovasc Interv Radiol 32:424–435
26. Ramsden JJ, Allen DM, Stephenson DJ et al (2007) The design and manufacture of biomedical surfs. CIRP Ann Manuf Technol 56:687–711
27. Hoche H, Scheerer H, Probst D et al (2003) Development of a plasma surface treatment for magnesium alloys to ensure sufficient wear and corrosion resistance. Surf Coat Technol 175:1018–1023
28. Tian XB, Wei CB, Yang SQ et al (2005) Corrosion resistance improvement of magnesium alloy using nitrogen plasma ion implantation. Surf Coat Technol 198:454–458
29. Wan GJ, Maitz MF, Sun H et al (2007) Corrosion properties of oxygen plasma immersion ion implantation treated magnesium. Surf Coat Technol 201:8267–8272
30. Zhao Y, Wu G, Pan H et al (2012) Formation and electrochemical behavior of Al and O plasma-implanted biodegradable Mg–Y–RE alloy. Mater Chem Phys 132:187–191
31. Morshed MM, Alam MM, Daniels SM (2011) Moisture removal from natural jute fibre by plasma drying process. Plasma Chem Plasma Process 32:249–258
32. Migliavacca F, Petrini L, Montanari V et al (2005) A predictive study of the mechanical behaviour of coronary stents by computer modelling. Med Eng Phys 27:13–18
33. Abderrazak K, Kriaa W, Ben Salem W et al (2009) Numerical and experimental studies of molten pool formation during an interaction of a pulse laser (Nd:YAG) with a magnesium alloy. Opt Laser Technol 41:470–480
34. Gray-Munro JE, Seguin C, Strong M (2009) Influence of surface modification on the in vitro corrosion rate of magnesium alloy AZ31. J Biomed Mater Res Part A 91:221–230
35. Nishimoto KT (2003) A study of plasma etching for use in active metals. MSc. thesis, Massachusetts Institute of Technology
36. Kim G-H, Kim C-I (2007) Dry etching of magnesium oxide thin films by using inductively coupled plasma for buffer layer of MFIS structure. Thin Solid Films 515:4955–4959
37. Hänzi AC, Gunde P, Schinhammer M, Uggowitzer PJ (2009) On the biodegradation performance of an Mg–Y–RE alloy with various surface conditions in simulated body fluid. Acta Biomater 5:162–171
38. Lu P, Cao L, Liu Y et al (2011) Evaluation of magnesium ions release, biocorrosion, and hemocompatibility of MAO/PLLA-modified magnesium alloy WE42. J Biomed Mater Res Part B 96:101–109
39. Seeger JM, Ingegno MD, Bigatan E et al (1995) Hydrophilic surface modification of metallic endoluminal stents. J Vasc Surg 22:327–336
40. Gu XN, Zheng YF (2010) A review on magnesium alloys as biodegradable materials. Front Mater Sci China 4:111–115
41. Yang J, Cui F, Lee IS (2011) Surface modifications of magnesium alloys for biomedical applications. Ann Biomed Eng 39:1857–1871
42. Gill P (2012) Corrosionand biocompatibility assessment of magnesium alloys. J Biomater Nanobiotechnol 03:10–13
43. Yi CH, Jeong CH, Lee YH et al (2004) Oxide surface cleaning by an atmospheric pressure plasma. Surf Coat Technol 177–178:711–715
44. Nakamura Y, Suzuki Y, Watanabe Y (1996) Effect of oxygen plasma etching on adhesion between polyimide films and metal. Thin Solid Films 290–291:367–369
45. Walter R, Kannan MB (2010) Influence of surface roughness on the corrosion behaviour of magnesium alloy. Mater Des 32:2350–2354
46. Kiousis DE, Wulff AR, Holzapfel GA (2009) Experimental studies and numerical analysis of the inflation and interaction of vascular balloon catheter–stent systems. Ann Biomed Eng 37:315–330